14th Australasian Fluid Mechanics Conference
Adelaide University, Adelaide, Australia
10-14 December 2001

Surface Pressure Measurements on a Group of Idealised Road Vehicle Models

F. Alam, G. Zimmer and S. Watkins
Automotive Engineering Group
Department of Mechanical and Manufacturing Engineering
RMIT University, Melbourne, Victoria, 3083, AUSTRALIA

Abstract

Aerodynamically generated noise in the A-pillar region of a passenger vehicle can make a significant contribution to interior noise and adversely affect passenger comfort. Many modern vehicles still have high fluctuating exterior pressures due to flow separations in this region. A series of experimental investigations were performed to study the effects of the A-pillar and windshield geometry on the local flow and its potential for noise generation using a group of idealized road vehicle models. Surface mean and fluctuating pressures were measured on the side window in the A-pillar region at different Reynolds numbers and yaw angles. Tests were carried out in RMIT Wind-Tunnel. Flow structure was documented using flow visualization. The studies show that Reynolds number sensitivities were minimal and the surface mean and fluctuating pressures can be scaled with velocity head and Strouhal number if no feedback mechanism is present. The magnitudes of the fluctuating pressure coefficients depend largely on local A-pillar radii and can be reduced significantly with the increase of local corner radii.

Introduction

Driving comfort of passenger vehicles is considered essential in markets throughout the world. One of the requirements pertains to the minimisation of aerodynamic noise. The aerodynamic noise is significant at driving speeds exceeding 100 km/h as structure-borne, engine, tyre, and power-train noise has been reduced over the last 20 years. High aerodynamic noise levels can not only make it difficult for vehicle occupants to converse or listen to the radio but also cause driver fatigue on a long highway trip. Studies by Watanabe et al. [6], Sadakata et al. [5], Haruna et al. [3], Popat [4] and Dobrzynski et al. [2] have revealed that the flow around a passenger car's A-pillar region is the primary source of aerodynamic noise, since the highest fluctuating pressure occurs here and it is the region closest to the driver's ears. However, the effects of A-pillar and windshield geometries on the potential for noise generation close to the A-pillar are not well published. The size and magnitude of the A-pillar flow separation mainly depend on the local A-pillar and windshield geometry and yaw angles. Although the pressure fluctuations arising from the A-pillar flow can directly cause acoustic wave generation, the main generator of in-cabin noise is considered to be from the vibration caused by the pressure fluctuation on the vehicle structures-generally the side glasses. CFD methods are not sufficiently developed to either predict the acoustic wave directly (although by analogy prediction can be attempted) nor the exact surface pressure fluctuations. One alternative to CFD methods for reducing research expenditure and time-to-market is to use scale models, which are instrumented to measure surface pressure fluctuations. The purpose of this paper is to investigate how these fluctuations vary with scale (Reynolds number) and also to document the effects of local geometry and yaw angles.

Idealised Vehicles Description

In order to study the effects of A-pillar and windshield geometry on the local flow, five 40% scale idealised vehicles (models) with different A-pillar and windshield geometry were made. The scale of the model was a compromise between minimising the blockage ratio and obtaining as close to full-size Reynolds number as possible. These models were kept simple without the added complication of wheels, wheel arches, engine compartment flow, side mirrors and fore-body details. In addition, models had no ground clearance and were parallel-sided in plan view. The variables were the A-pillar/windshield curvature, Reynolds number (varied by tunnel speed), yaw angle and windshield inclination angle. Each of the five models were made with a different A-pillar/windshield curvature: a semi-circular shape, a small semi-ellipsoidal shape, a large semi-ellipsoidal shape, a slanted sharp-edged shape all with 60° flat windshield inclination angles, and a sharp-edged vertical windscreen shape. More details about the model geometry can be found in the Ph.D. thesis by Alam [1].

Test Procedure and Data Processing

Experiments were performed using scale models with different A-pillar/windshield geometries at RMIT University Industrial Wind-Tunnel. The surface mean and fluctuating pressures were measured at speeds of 60, 80, 100, 120 and 140 km/h and under different yaw angles (±15° in increments of 5°) for all scale models. In order to obtain a comprehensive pressure distribution, 32 pressure holes were drilled normal to the window surface in two rows for each top section of the model. The bottom row was approximately 1/3 distance away from the baseline of the window and the top row was 2/3 the distance from the window base. Each row carried 16 holes. The space between any two adjacent holes was 32 mm. Before drilling the holes, flow visualisation was carried out to determine flow in the area of interest (i.e., the region that is influenced by the A-pillar vortex).

A 48 channel Scanivalve pressure measurement unit was used to scan the surface mean pressure. The time-averaged pressure distributions were then converted to the non-dimensional pressure coefficients (Cp) using the following relation: $C_p = \frac{p_m - p_\infty}{\frac{1}{2}\rho V_\infty^2}$.

Here p_m is the time-averaged surface pressure on the side window near the A-pillar), p_∞ is the free stream static pressure and V_∞ is the free stream velocity. Two ¼ inch condenser microphones were used to measure the fluctuating surface pressure. Microphones were connected to a 16 channel Digital Audio Tape recorder through preamplifiers and power modules. All microphones were calibrated before and after the measurements via a pistonphone calibrator. A 10-second sample out of a 30-second sample obtained at 48,000 Hz was analysed to calculate the non-dimensional fluctuating pressure coefficients (Cp rms) using the following relationship ($C_{p\,rms} = \frac{p_{std}}{\frac{1}{2}\rho V^2}$), where p_{std} is the standard deviation of the fluctuating pressure and $\frac{1}{2}\rho V^2$

is the mean velocity head (q). The mean velocity head was obtained from the tunnel data acquisition system.

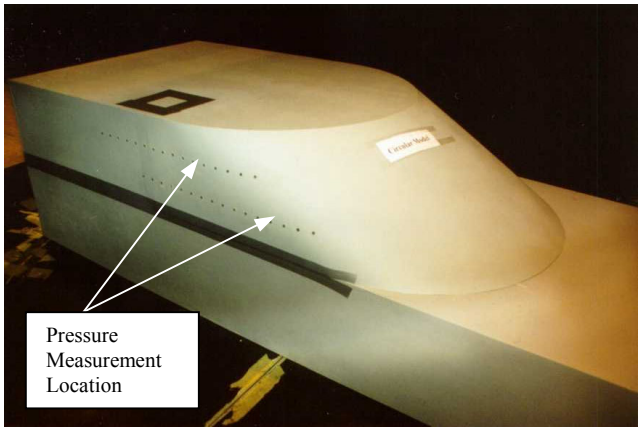

Figure 1: Large Ellipsoidal Model Showing the Location of Pressure Measurements

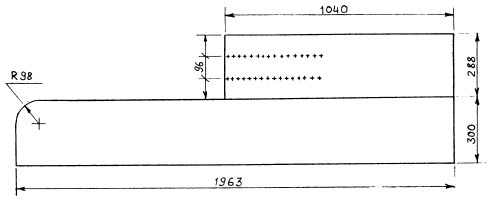

a). Front View (Rectangular Model)

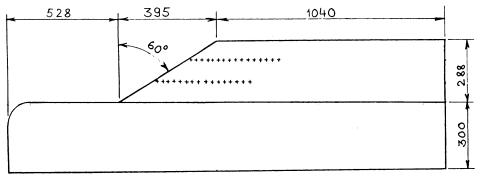

b). Front View (Slanted Sharp-edged Model)

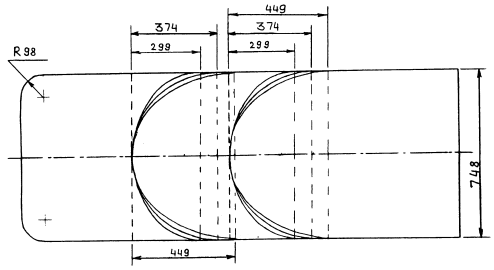

c). Top View (all five models)

[Rectangular, Slanted Sharp-edged, Small Ellipsoidal, Circular and Large Ellipsoidal Models]

Figure 2: External Dimension of Idealised Models

Due to strong pressure fluctuations in the A-pillar region on the side window of the sharp-edged model and rectangular model, the fluctuating pressure was only measured at three speeds (60, 80 and 100 km/h) in order to avoid the microphones over-ranging. However, the fluctuating pressure for other three models have been measured at all speeds.

Results and Discussion

The surface mean and fluctuating pressure coefficients are plotted against the distance from the line of symmetry (at the front) of models (for details of how the graphical results relate to the model geometry, refer to the Ph.D. thesis by Alam [1]. For compactness, when non-zero yaw angle data are presented, data from the upstream and downstream side are plotted on the same figure.

Effects of Reynolds Numbers and Yaw Angles on Surface Mean and Fluctuating Pressures

The surface mean and fluctuating pressure coefficients for the slanted sharp-edged model are shown in Figures 3 to 6. Figures 3 and 4 show the mirror image of surface mean and fluctuating pressure distributions to the left and right hand sides of the slanted sharp-edged model for zero yaw angle. Figures 5 and 6 demonstrate the mean and fluctuating pressure distributions along the leeward side window (-15° yaw angle) and windward side window (+15° yaw angle) for the same model. The plots for other models (not shown here due to space limitation) show that the surface mean pressure coefficients are virtually independent of Reynolds numbers for all models at zero, -15° and +15° yaw angles. However, a small variation of Cp is evident at the most negative values of Cp (thought to be close to the middle of the A-pillar vortex) at negative yaw angles. The surface fluctuating pressure coefficients for all models are virtually independent of Reynolds numbers at zero, -15° and +15° yaw angles. However, a small variation is evident in separated zones at lower Reynolds numbers (between 60 km/h and higher speeds). This may be due to minor experimental error.

Yaw angles have significant effects on the magnitude and size of the A-pillar flow separations. For the rectangular (not shown here) and slanted sharp-edged models, the locations of the maximum magnitudes of the Cp and Cp rms move downstream from the A-pillar leading edge with increasing negative yaw angles. The area of separated zones at positive yaw angles reduces significantly compared to negative yaw angles although, surprisingly, the magnitude of pressure fluctuations increases with positive yaw angle for the rectangular model. No flow separation is evident at zero, negative and positive yaw angles for the large ellipsoidal and circular models. Minor separation is noted for the small ellipsoidal models at negative yaw angles and it appears that the separation pattern is complex (i.e., there are double peaks in some of the mean and fluctuating pressure distributions). At positive yaw angles, a small but strong flow separation is evident for the rectangular model. Flow visualisation photographs (not shown here) support these observations.

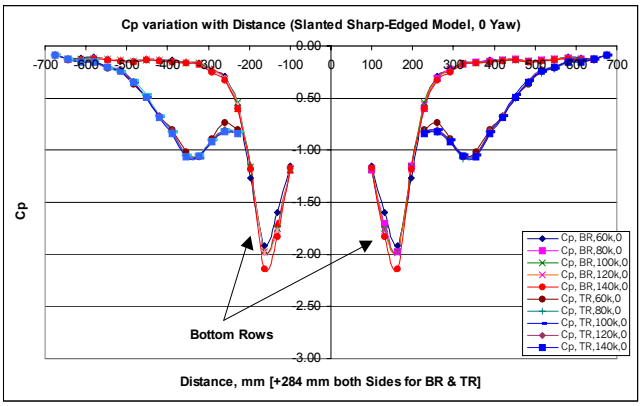

Figure 3: Surface Mean Cp Variation with Distance, Yaw = 0° (Slanted Sharp-edged Model)

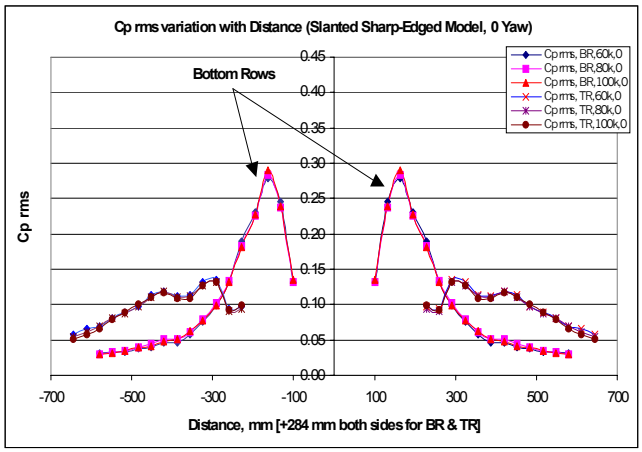

Figure 4: Surface Fluctuating Cp rms Variation with Distance, Yaw = 0° (Slanted Sharp-edged Model)

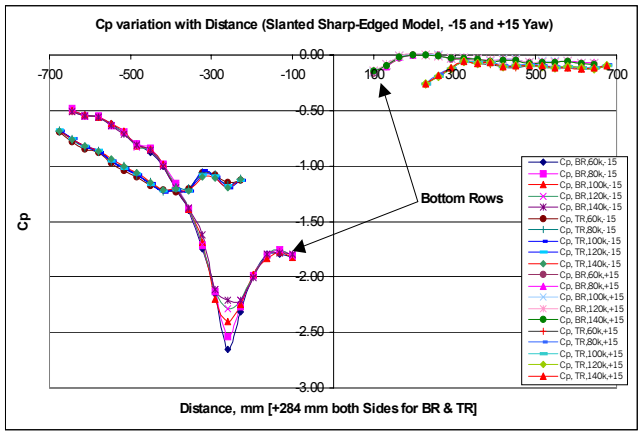

Figure 5: Surface Mean Cp Variation with Distance, Yaw = -15° and +15° (Slanted Sharp-edged Model)

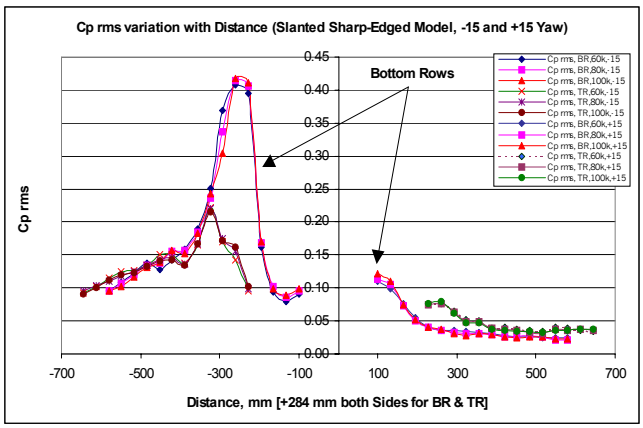

Figure 6: Surface Fluctuating Cp rms Variation with Distance, Yaw = -15° and +15° (Slanted Sharp-edged Model)

Spectral Analysis

Power Spectral Density (PSD) was used to document the energy characteristics of signals in the frequency domain. The fluctuating pressure data from the position where the maximum fluctuating pressure, (measured at zero and ±15° yaw angles) was used for PSD analysis and plotted against the frequency and Strouhal number. Except where stated the test velocity was 100 km/h. The vertical axis (pressure squared) of the power spectrum was normalised by dividing by the velocity head (q). The Strouhal number is given by, $S_t = \frac{fL}{U}$, where L is a characteristic length scale of the separation and U is the local velocity and f is the frequency. The characteristic length scale (L) is frequently the boundary layer displacement thickness (when no flow separation exists), however in separated flow fields, the boundary layer displacement thickness (L) is no longer relevant. Instead, a characteristic disturbance scale needs to be selected. It is sometimes difficult to determine the appropriate length scale and in those cases L=1 meter is generally accepted. In this study, the spectral density was normalised using L=1 m.

The PSD, plotted against frequency at the locations of negative, zero and positive yaw angles (-15°, 0° and +15°) for the slanted sharp-edged model is shown in Figure 7. The normalised PSD plot at zero yaw angle for the same model is shown in Figure 8. The power spectral density plot shows that the energy content is higher in the separated regions compared to the unseparated regions. The negative yaw angle contains more energy compared to zero and positive yaw angles. Most energy in separated regions of the A-pillar vortex is in frequencies below 400 Hz and the peak energy is usually below 200 Hz. However, the peak shifts with yaw angle. Although the spectral energy in unseparated regions remains higher in frequencies up to 3000 Hz, the magnitude is much smaller compared to the spectral energy in separated regions (i.e., this energy is from the turbulent boundary layer). The normalised PSD plots for other models (not shown here) show that all spectral curves at different speeds generally collapse onto a single curve. However, a small variation is evident at Strouhal numbers below about 25 for the small ellipsoidal model and about 170 for the large ellipsoidal models. No apparent variation is noted for the slanted sharp-edged model where the flow separation points are fixed. If the normalised pressure spectra collapse onto a single curve, the spectra can be used to extrapolate pressure fluctuations at speeds that were outside the test range. Spectra generally collapse onto a single curve if the noise is broad band in nature. Most noises generated in the A-pillar region are of the broad band type. The normalised spectra are also used to assess the effects of Reynolds numbers. The normalised spectra at different speeds under constant yaw angles for all scale models show that all spectra collapse onto a single curve except for some minor variations mentioned earlier.

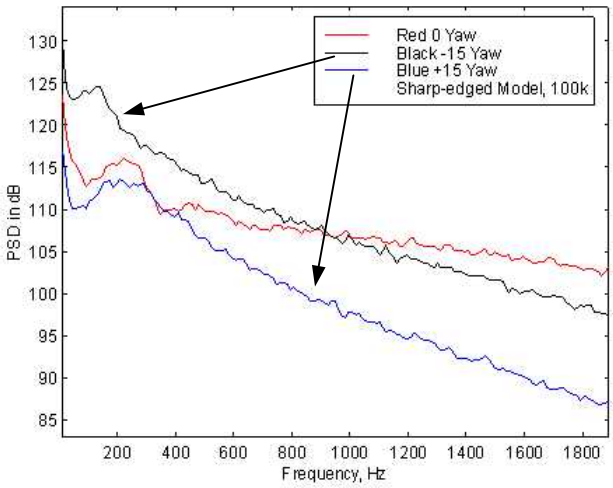

Figure 7: Slanted Sharp-edged Model, Effects of Yaw

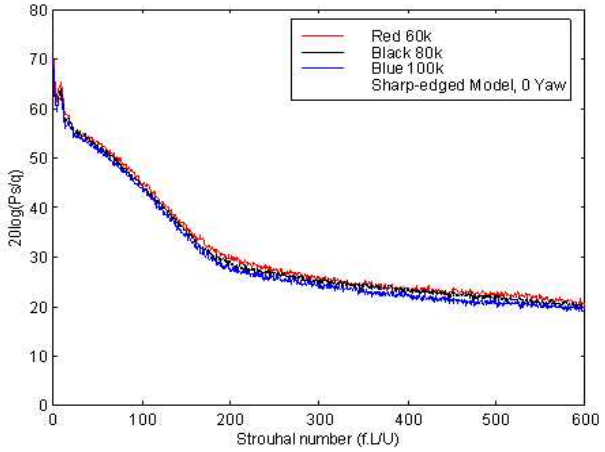

Figure 8: Slanted Sharp-edged Model, Effects of Velocity, Zero Yaw

Effects of Shape (A-Pillar/ Windshield Curvatures) on Fluctuating Pressures

In order to compare the fluctuating pressures as a function of shape, data for all models at zero yaw angles are presented in Figure 9 and for –15 and +15 yaw in Figure 10. Only the data at 100 km/h from bottom row are presented in Figures 9 and 10 since this was the location of maximum fluctuating pressures. The radius of local A-pillar for the small and large ellipsoidal models was 250 mm and 500 mm respectively and for the circular model was 375 mm. Figures 9 and 10 show how the peak Cp rms varies with local curvatures.

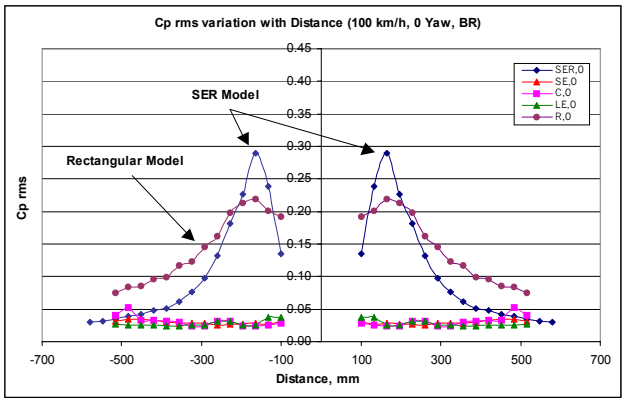

Figure 9: Fluctuating Cp rms Variations with Distance, Yaw = 0° (All Models)

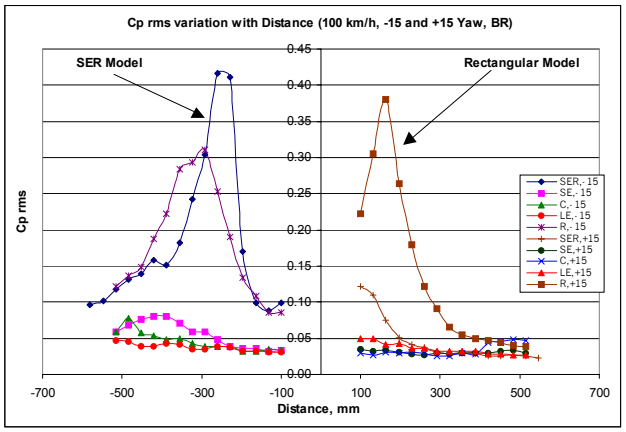

Figure 10: Fluctuating Cp rms Variations with Distance, Yaw = -15° and +15° (All Models)

For negative and zero yaw angles the slanted sharp-edged model has the highest Cp rms and the rectangular model has the second highest value of Cp rms. However, the fluctuating pressure is reducing significantly with increased A-pillar/windshield radius. The highest fluctuating pressure coefficient is noted for the rectangular model that represents a vertical windscreen at zero yaw angles.

Conclusions

- The surface mean and fluctuating pressure coefficients are independent of Reynolds numbers for scale models at positive yaw angles and slightly dependent on Reynolds number at negative and zero yaw angles. The normalised power spectral density demonstrates no significant effect of Reynolds numbers.
- The frequency-based analysis indicates that most energy from the pressure fluctuation in the A-pillar region lies between 100 and 400 Hz and the peak energy is close to 200 Hz.
- Model-scale data give a good indication for extrapolation to full-scale vehicle as pressure coefficients and normalised spectra are independent of Reynolds numbers.
- The surface mean Cp and fluctuating Cp rms plots in conjunction with the flow visualisation, show that the maximum hydrodynamic pressure fluctuation occurs in between the separated and re-attached areas.
- The positive yaw angle reduces the area and magnitude of the flow separation and the negative yaw angle increases the area and magnitude of the flow separation. However, a vertical windshield is capable of producing an intense but relatively small flow separation at positive yaw angles.

Acknowledgments

The Authors express their sincere thanks to the Australian Federal Government for providing the financial assistance to first and third authors through the Australian Postgraduate Award (APA) scholarships.

References

[1] Alam, F., “The Effects of Car A-pillar and Windshield Geometry on Local Flow and Noise”, Ph.D. Thesis, Department of Mechanical and Manufacturing Engineering, RMIT University, Melbourne, Australia, September, 2000.

[2] Dobrzynski, W. and Soja, H., “Effect on Passenger Car Wind Noise Sources of Different A-Post Configurations”, Inter-Noise-94, PP 387-390, Yokohama, August 29-31, 1994, Japan.

[3] Haruna, S., Nouzawa, T., Kamimoto, I. and Hiroshi, S., “An Experimental Analysis and Estimation of Aerodynamic Noise Using a Production Vehicle,” SAE Paper No. 900316, 1990.

[4] Popat, B. C., “Study of Flow and Noise Generation from Car A-pillars”, Ph.D. Thesis, Department of Aeronautics, Imperial College of Science, Technology and Medicine, The University of London, U.K, 1991.

[5] Sadakata, O., “A Consideration of Wind Noise Reduction by Air Flow Control”, 22nd FISITA No. 885115, PP 182-189, 1988.

[6] Watanabe, M. and Harita, M., “The Effects of Body Shapes on Wind Noise”, SAE Paper No. 780266, 1978.